Mr. Manjunath Raikar. International Journal of Engineering Research and Applications
www.ijera.com
ISSN: 2248-9622, Vol. 10, Issue 9, September, 2020, pp: 55-62

RESEARCH ARTICLE OPEN ACCESS

Conceptual Structure for Oxide Ceramic's Dislocation-Modified Conductivity Deconvoluting Space Charge, Core, and Mesoscopic Structure as Applied to $SrTiO_3$

Mr. Manjunath Raikar
Lecturer / Department of Electrical & Electronics
Sri Channakeshava Govt Polytechnic - Bankapur-581202, Dist Haveri
manjunathraikarn@gmail.com

Date of Submission: 08-09-2020 Date of acceptance: 22-09-2020

ABSTRACT
One recently suggested tactic to modify ceramics' functional and particularly electrical characteristics is the insertion of dislocations. Although several investigations verify that dislocations have a discernible effect on electrical conductivity, some express apprehension when studying dislocation configurations that extend beyond a bicrystal interface that is geometrically tractable. Furthermore, the design of dislocation-modified electrical conductivity is hampered, and a systematic debate is complicated by the absence of a comprehensive categorization on relevant dislocation properties. We next continue to mechanically introduce dislocations with three distinct mesoscopic structures into the single-crystal SrTiO3 model material, and we thoroughly characterize them from both an electrical and mechanical point of view [3]. Ultimately, by deconvolution Ing mesoscopic structure, core structure, and space charge, we can get a comprehensive understanding of how dislocations affect functional qualities, with an emphasis on electric properties.

Keywords: Dislocations, Plastic Deformation, one-dimensional, conductivity, doping, ceramics, oxides

I. INTRODUCTION

Reviews of the oxides2 and alkali halides1 show that, even though dislocations are often discussed in a mechanical context, they can affect the functional qualities of ceramics. Analysis is greatly complicated by the multiplicity of cooperative and competing conductivity processes, and it is sometimes unclear how they relate to one another. For instance, several processes involving dislocations can alter the electrical conductivity of electronically insulating materials, which is often largely ionic conductivity. One way to improve it is by increasing mobility along the core, as explained by ionic pipe diffusion, or by increasing charge carrier concentration since the undisturbed lattice's stoichiometry differs from the cores [1]. However, there is a space charge zone that compensates for the charged dislocation core. This could also function as an extra transport channel or barrier. Furthermore, it is important to consider local point defect concentrations and the potential enhancement of ionic conductivity by the tensile strain field surrounding a dislocation.

Thus far, it has been determined that, for example, at low-angle tilt borders in $SrTiO_3$, oxygen transport is impeded perpendicular to dislocation networks. Oxygen vacancies (and other positive defects, such as holes) are eliminated from the negative space charge layer around the positively charged core. The decrease in vacancy concentration thus acts as a potential barrier for oxygen vacancy transfer caused by overlapping space charges. Moreover, it was shown that strontium titanate's naturally occurring surface space charge layer may be extended by a dislocation-rich area. It is proposed that a high dislocation number density imitates electrical characteristics like acceptor doping. For this reason, the process of adding dislocations to electro ceramics was specifically referred to as one-dimensional doping [2].

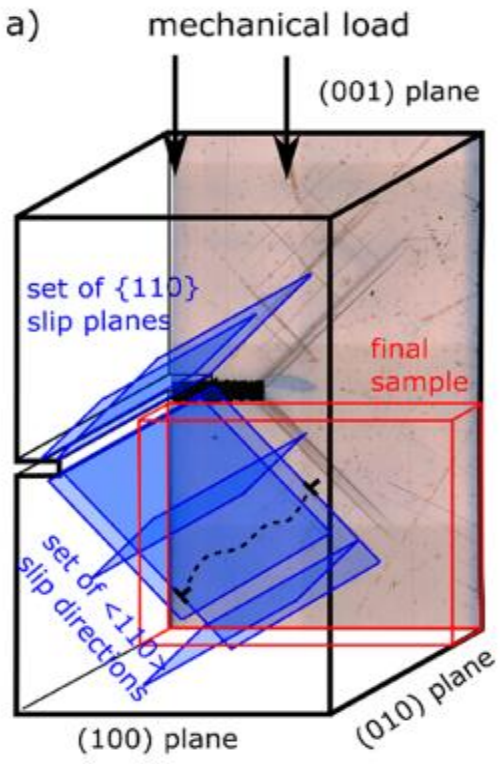

Figure No. 1 - Diagrammatic representation of directed $SrTiO_3$ deformation

Understanding of bicrystal interfaces has progressed significantly, and they are a great model system for characterizing well-aligned networks of dislocations. This has been the chosen dislocation configuration for modeling investigations as well as transmission electron microscopy (TEM). We go beyond crystalline interfaces in this study by incorporating complicated dislocation configurations into our conceptual framework. An industrially scalable technique called plastic deformation produces a wide variety of extremely complicated mesoscopic dislocation structures and arrangements, many of which have connected effects that make it challenging to comprehend any one consequence separately. The influences of space charge and core charge combine to complicate the arrangement's electrical characteristics. Distinguishing the prominent impacts is necessary for a mechanistic understanding.

Several crystal structures are intriguing for their potential to be used in dislocation-based functionality tailoring. Comprehensive analyses of LiF, and $SrTiO_3$ and TiO_2, demonstrate the promise of this approach. There may be several intriguing candidate materials included in a single crystal structure. Dislocations within a single ceramic can affect several functional parameters, including the electrical and thermal conductivity of $SrTiO_3$. 26 Additional instances of altered attributes include ionic conductivity (titanium in $Al2O_3$ and oxygen in YSZ),

Keep in mind that relative impacts often increase with suitable (low, for example) intrinsic defect concentration. Regarding its defective chemistry, strontium titanate is a ceramic material that has been well studied. However, it also piques curiosity for its advanced functionality, such as resistive switching, where debates over the effects of dislocations have been sparked. It is still not well understood how dominant processes, such as improved conductivity along the dislocation core (or lack thereof), are mediated, and effects could be correlated [4].

II. PROPOSED SYSTEM

Three distinct dislocation arrangements—all made possible by mechanical deformation—are compared in this work to filter influencing factors. High-voltage electron microscopy and dark-field X-ray microscopy are used to examine the inserted mesoscopic dislocation formations. Additional information to the arrangement analysis comes from atomic resolution photographs of the core. Temperature and partial pressure-dependent impedance spectroscopy observations are used to produce Arrhenius plots, activation energies, and sections of a Brouwer diagram showing the electrical conductivity with and without dislocations. The difference in oxygen transport between the bulk of deformed single-crystalline strontium titanate and dislocation-rich sections is clarified with the use of oxygen tracer diffusion studies on SrTiO3 carried out by time-of-flight secondary ion mass spectrometry (ToF-SIMS) [5].

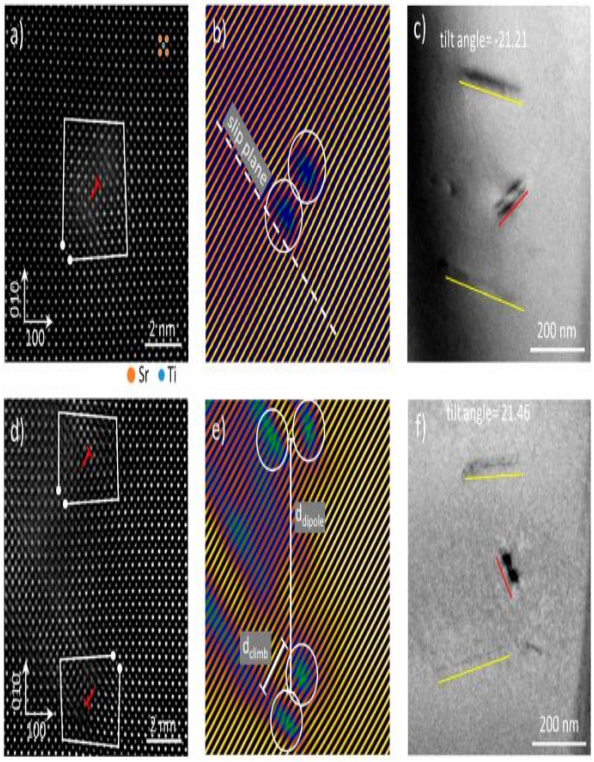

Figure No. 2 - The dislocation core of 100 type dislocations implanted at ambient temperature was examined using atomic resolution thermal imaging.

The 100 slip systems are activated by controlled uniaxial plastic deformation at high and low temperatures, respectively, in contrast to simple polishing, which maximizes the dislocation density. The mesoscopic structure and arrangement are demonstrated to have a significant influence on the dislocation-induced effect on conductivity, which was not evident in the first two examples but was evident in the third. Therefore, it is far too general to draw desirable simple generalizations like "dislocations are conductive" or even "mechanically introduced dislocations in $SrTiO_3$ impact conductivity." A framework for describing the mesoscopic and nanostructure, defect chemistry, and dislocation characteristics in ceramics is produced by this approach. Consequently, it helps to disentangle the effects of the dislocations' space charge, core, and mesoscopic structure [6].

III. METHODOLOGY

Single crystals of $SrTiO_3$ doped with acceptor (0.05 weight percent Fe) were cut in either the [001] or [110] directions. For the room-temperature mobile slip system {110}, the [001] loading orientation maximizes the Schmid factor (quantification of resolved shear stress on prospective glide plane as a function of angles between load direction, slip plane, and slip direction yields a propensity for plastic deformation). The Schmid factor for the high-temperature slip system {100} is maximized in the [110] orientation. Keep in mind that the two systems' dislocation multiplication processes differ from one another. In the low-temperature 100 slip system, bundles of dense parallel dislocation bands emerge; in contrast, the dislocations caused by high-temperature deformation, where {100} is the active slip system, are uniformly dispersed throughout the sample. These approaches may be used to obtain samples, regardless of the slip systems, where the induced dislocations in the electrical analysis or diffusion studies lie along or perpendicular to the measurement direction. Therefore, it may be inferred that, as shown, dislocations in extracted samples stretch from top to bottom. Thus, it seems possible to test the electrical characteristics along the dislocations. Since Figure 1 only shows a two-dimensional picture of the produced dislocations mesoscopic structure, additional structural research was done to confirm that an ordered network is obtained from top to bottom in the sample.

Type dislocations were studied using dark-field X-ray microscopy (DFXM), which allows for the identification of individual dislocations in large volumes. In electrical tests, the likelihood of dislocations generating percolating electrical channels from the bottom to the top surface is highest when they span multiple 10−100 μm. Cross slip components are also present. It's interesting to note that neither the dislocation lines nor the edge character seems to be pure screw. Because of this, the dislocation arrangement is very different from dislocations studied in bicrystalline crystals. This is somewhat consistent with polycrystalline strontium titanite findings. Figures 2 show the results of ultrahigh voltage electron microscopy (UHVEM) on Verneuil produced crystals, which show dislocations in the corresponding high-temperature and low-temperature slip planes. The dislocation lines have kinks and jogs in addition to being not quite straight. The distance between the dislocations also varies. Moreover, tiny loops and dislocation dipole segments may be seen. The dislocations seem to be mostly loops restricted to several 10 μm extensions, especially for the high-temperature slip system [7].

Details about the dislocation core are just as crucial as the mesoscopic structure of dislocations. Since {100}-type dislocation cores have already been documented in the literature, dislocations of the {110} slip system that were extracted from a slip band using a focused ion beam were subjected to atomically resolved high-angle annular dark-field scanning transmission electron

microscopy (HAADF-STEM). Figure 3a shows the Fourier transformed picture of the lattice planes shown in Figure 3b, together with a typical [10] edge dislocation inside a slip band. As is also observed in polycrystalline samples50 and for pure edge-type dislocations from modeling, the core is divided into two partial dislocations. Nevertheless, as the schematic in Figure S4 of the Supporting Information also shows, the partial dislocations are in a relatively separated position. It is quite probable that the energy input from the electron beam is what causes the climb dissociation. When the partial dislocation is exposed to an electron beam, it begins to migrate toward the climb dissociated position. This is also true when thermal activation takes place. Above 700 °C, the dislocation dipole structure that is common for deformation at ambient temperature becomes thermally unstable (see Figure in the Supporting Information). Two dislocation cores (each divided into two parts) with opposing line vectors and similar Burgers vectors can be seen in Figure 3d, generating a close-knit dipole. This characteristic is not present in bicrystals [8].

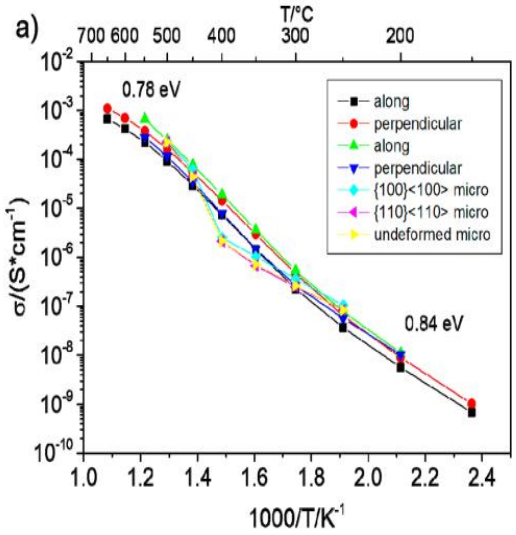

Figure No. 3 - Arrhenius plot showing electrical measurements made on bulk and microelectrode samples in air.

The observation from DFXM is further supported by the fact that, upon sample tilt, dislocations do not extend straight along the edge direction (see Figure 3c, f). Just 15 μm behind the tip of a band, a complex structure with several mixed character sections and dipoles can be seen. At the tip of a band, the edge character can be primarily seen with UHVEM (see Figure 2b) [7]. Firstly, as shown in Figure 3b, dipoles are already present near the extremity of the band that is indicated by arrows. Therefore, the {110} dislocations in single crystals that are mechanically generated divide into partial dislocations that are quite different from the {110} dislocations in bicrystals. The results on polycrystalline material bear parallels with the findings, indicating that the mixed character occurs naturally in the bulk. The data originates from the upper few nm of the sample since the final picture is sensitive to the focus plane during imaging. As a result, even when the dislocation line is not parallel to the beam, atomic resolution photos were nevertheless achievable for most observations. Because of the tilt of the atom columns, Figure 3d shows the bonds around dislocation lines extended along the [110] direction. It's also possible for the dislocation line near the surface to somewhat reorganize. According to the UHVEM observations, the dislocations frequently result in the formation of dipoles (Figure 3d, e). Since the lateral extension is almost equal to the lamella thickness, this set of TEM data really shows a [110] orientation of the dislocation core through the TEM lamella thickness [9].

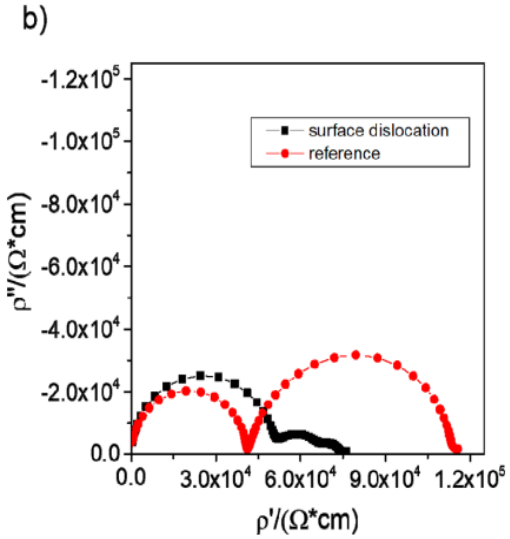

Figure No. 4 - Nyquist plots of the resistivity from impedance spectra of an undeformed reference SrTiO3 single crystal at 450 °C

The variations in how the three dislocation layouts affect conductivity will be explained in the sections that follow. The charge of the core and the associated space charge are unknown as there are no TEM or modeling investigations for the reported mixed dislocation cores. Moreover, it is unlikely that dislocations of the type penetrate through the samples from top to bottom. In addition, every dislocation displays unique characteristics such dipoles, jogs, and kinks. Their effect on charge transport and electrical characteristics is unpredictable. However, it is anticipated that

overlapping space charges are important for charge transmission, at least for pure edge and pure screw-type dislocations. If dislocations do not completely span from top to bottom of a sample, a conductive channel (or blocking layer) might nevertheless form due to an overlap of space charges [10].

When measuring along the dislocation line, a low-angle tilt grain boundary in a dislocation spacing of 5nm would be found below an electrode of 200 × 200 μm^2, according to a quantitative comparison of the dislocation density to bicrystals in the case of a volume with a density of 1012 m^{-2}. These are quite modest when compared to the dislocation damage of 1015 m^{-2} (average distance 30 nm) obtained by rough polishing. ***De Souza et al. (2005)*** observed that when the cores are closer than 5−10 nm, space charges overlap significantly. In this instance, the space charge zone's extent is greater than half the separation between the dislocations. Once more, because this figure was calculated for a specific arrangement and core defect chemistry with a specific doping and bulk thermal treatment, it should only be extrapolated to other investigations with caution.

The conductivity of samples with dislocations parallel to and along the direction of the electric field is shown on an Arrhenius plot, as shown in A. For all samples, there is a departure from the typical linear slope at higher temperatures, which is explained by the dominating charge carriers switching from oxygen vacancies to holes. Based on impedance spectroscopy, the capacitance of the resistive process under investigation is within the range of 1 × 10−11 F. Consequently, a bulk process might be responsible for the electrical response.56 It is discovered that the conductivity is about the same for every sample considered. The activation energies for the high-temperature regime (0.78eV) and low-temperature regime (0.84eV) could be derived, apart from the transition area (about 300–450 °C). Additionally, these values are the same throughout the examined samples. These findings show that the electrical characteristics are not significantly affected by a dislocation density of 1012 m^{-2} of 100⟩{100} type or 2 × 1013 m^{-2} of ⟨110⟩{110} type. Additionally, a second response in the impedance experiment with a field perpendicular to the layer (not shown) does not reveal a blocking effect of dislocations [12].

IV. FINAL RESULT

We employ 18_O tracer studies to further explore the space charge zone and validate our findings using a complementary method. The dislocations created in this study are parallel to the tracer's diffusion direction because they reach into the bulk on the (110) plane. F-SIMS may be used to examine mechanically generated dislocations that create large dense patches on parallel slip bands (Figure 1) in contrast to low-angle tilt boundaries. It is far more probable to identify the impact of regions with parallel bands of dislocations at a surface resolution of around 100 nm. It should be noted that prior to the O tracer exchange trials, an HF etching phase was also carried out. A UV-sensitive polymer was coated in a stripe pattern onto the surface before the etching process to assess, using lithography, the difference in oxygen incorporation between etched and unetched areas. As a result, areas were alternately etched and unetched (Figure 1d).

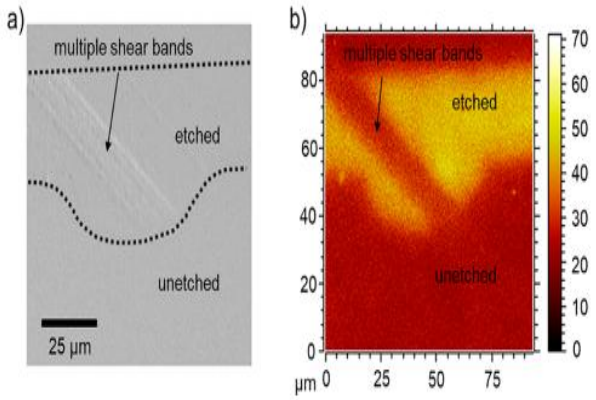

Figure No. 5 - secondary electron picture of the area of interest showing the various sections

A secondary electron picture of a region of interest produced by primary ions in the ToF-SIMS is shown in Figure 5a. The matching picture in Figure 5b shows the isotope ratio 18_O* lateral distribution, which is determined by

$$x^*_{18_o} = \frac{I_{18_o}}{I_{18_o} + I_{16_o}}$$

where I_{18O} and I_{16O} are the corresponding secondary ion intensities of 18_O and 16_O.The 18_O ratio in the isotope-enriched gas (x_{gas} = 0.97) and the natural abundance of 18O (x_{bg} = 0.0021) can be used to normalize the ratio.

$$x^*_{18_o} = \frac{x^*_{18_o} - x_{bg}}{x_{gas} - x_{bg}}$$

However, in the current instance, this has no effect on values. Figure 5b's color scale on the right shows how the 18_O concentration rises from bottom to top. All the intensities are gathered by depth profiling around 1 μm into the sample. It is therefore the total of all measurements of the region of interest that have been documented. There are discernible variations in $x18_O$ in regions with varying surface treatment or dislocation density (Figure 5a, b). The etched region may be divided

into two distinct sections after being treated with an HF buffer solution: one with a high density of dislocations and one without. The various shear bands in parallel that are seen in Figure 5a are clearly contrasted. It appears that there is less tracer incorporation and diffusion into the unetched region than into the etched zone (Figure 5b). This is consistent with findings from earlier studies that show how $SrTiO_3$ blocking surface space charge area may be altered, increasing the amount of oxygen that can be etched into the bulk material. Strontium-rich phases that alter the Sr/Ti ratio at the surface are most likely eliminated. Nonetheless, there is no appreciable rise in oxygen incorporation in the etched region in the high dislocation density zone. This demonstrates a basic distinction in the assimilation or diffusion of oxygen in the corresponding regions.

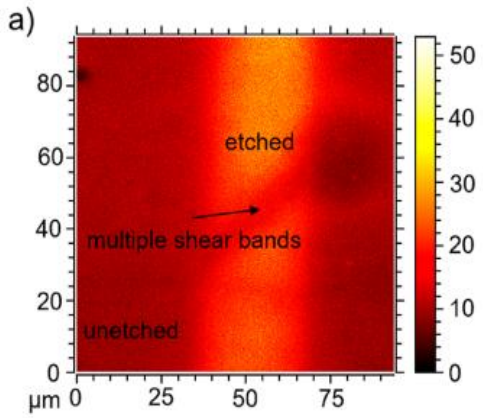

Figure No. 6 - Lateral image of x18O from depth profiling in ToF-SIMS

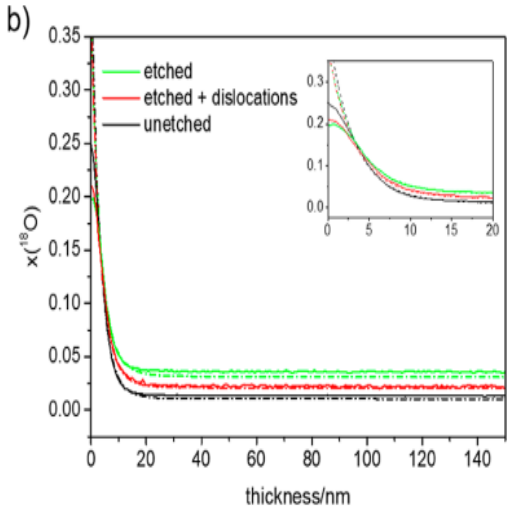

Figure No. 7 – The annealing temperature for the tracer experiment was 650 ^{0}C

secondary ions in conjunction with a suitable lateral resolution to enable effective imaging. For $x18_O$, analogous findings are shown in Figure 6a. The dislocation-free etched zone has a greater tracer concentration than the unetched or etched dislocation-rich region, which has a lower content. The measurement shown in Figure 5a's related $x18_O$ depth profiles are shown. To quantify the behavior at the surface, just the first 150 nm of depth are examined. The surface space charge layer (up to approximately 15 nm depth) affects the initial portion. A strongly blocking space charge barrier that is inhibiting transport into the bulk is suggested by a large buildup of 18_O tracer species near the surface [13].

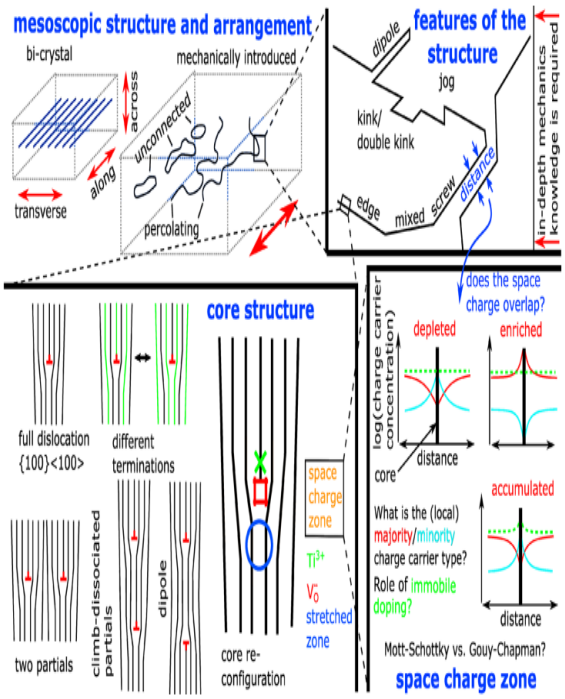

Figure No. 8 - The framework's constituent parts that explain dislocation-induced functionality

The formation of distinct terraces from surfaces with varying orientations in relation to the (100) surface provides an explanation for the etch pits' varying surface potential. Different terminations from preferential etching may produce variances in surface inclusion. It has also been demonstrated that such effects affect photoelectric characteristics [14].

Thus, the behavior previously attributed to dislocations may be caused by a severe influence on systems associated to oxygen transport. For instance, varying surface characteristics may be the cause of filamentary resistive switching phenomena in etc pits or mechanically deformed surfaces. As neither oxygen nor electronic transport is enhanced,

enhanced resistive switching, as it was seen at grain boundaries in SrTiO3, should not be seen for these kinds of dislocation. Strongly decreasing circumstances are often the cause of filamentary resistive switching. Even though the investigation only looked at oxidizing and slightly reducing circumstances, it might nevertheless add to the conversation on the potential impact of dislocations on filamentary resistive switching processes [15].

V. CONCLUSION

The mesoscopic structure of the ceramics (alignment, density/distance, type, orientation, propensity to form partial dislocations and loops/kinks), the charge and structure of their core, the surrounding space charge, and the defect chemistry of the bulk all influence the functional property changes brought about by the introduction of dislocations. In single-crystal SrTiO3, dislocations brought about by controlled uniaxial mechanical deformation create a complicated structure that includes dipoles and a mixed type for the {110} low temperature slip system. The {100} high-temperature slip system, on the other hand, creates disconnected loops. Temperature and oxygen partial pressure dependent conductivity were not seen to alter. On the other hand, compared to controlled bulk deformation, the electrical characteristics of $SrTiO_3$ are significantly affected by the introduction of a large density of disordered surface dislocations.

Apart from the increasing density, several additional impacting variables cannot be ruled out just yet. These are the characteristics of dislocations (mixed vs. edge, for example), core reconfigurations (glide vs. climb disconnected), or dopant or impurity segregations. As a result, the capacity to introduce dislocations into ceramics and modify their functional qualities depends on the ability to concisely manage their mesoscopic structure, which affects both the ensuing space charge and the core structure and charge.

REFRENCE

[1]. Nakagawa, T.; Nakamura, A.; Sakaguchi, I.; Shibata, N.; Lagerlof, K. P. D.; Yamamoto, T.; Haneda, H.; Ikuhara, Y. Oxygen Pipe Diffusion in Sapphire Basal Dislocation. J. Ceram. Soc. Jpn. 2006, 114, 1013−1017.

[2]. Noll, F.; Münch, W.; Denk, I.; Maier, J. SrTiO3 as a Prototype of a Mixed Conductor. Conductivities, Oxygen Diffusion and Boundary Effects. Solid State Ionics 2020, 86−88, 711−717.

[3]. Moos, R.; Hardtl, K. H. Defect Chemistry of Donor-Doped and¨Undoped Strontium Titanate Ceramics between 1000 Degrees and 1400 Degrees C. J. Am. Ceram. Soc. 2018, 80, 2549−2562.

[4]. Merkle, R.; Maier, J. How Is Oxygen Incorporated into Oxides? A Comprehensive Kinetic Study of a Simple Solid-State Reaction with Srtio3 as a Model Material. Angew. Chem., Int. Ed. 2008, 47, 3874− 3894.

[5]. De Souza, R. A. Oxygen Diffusion in SrTiO3 and Related Perovskite Oxides. Adv. Funct. Mater. 2015, 25, 6326−6342.

[6]. Waser, R.; Dittmann, R.; Staikov, G.; Szot, K. Redox-Based Resistive Switching Memories - Nanoionic Mechanisms, Prospects, and Challenges. Adv. Mater. 2009, 21, 2632−2663.

[7]. Wojtyniak, M.; Szot, K.; Wrzalik, R.; Rodenbücher, C.; Roth, G.; Waser, R. Electro-Degradation and Resistive Switching of FeDoped SrTiO3 Single Crystal. J. Appl. Phys. 2013, 113, No. 083713.

[8]. Kubicek, M.; Taibl, S.; Navickas, E.; Hutter, H.; Fafilek, G.; Fleig, J. Resistive States in Strontium Titanate Thin Films: Bias Effects and Mechanisms at High and Low Temperature. J. Electroceram. 2017, 39, 197−209.

[9]. Wang, J.-J.; Huang, H.-B.; Bayer, T. J. M.; Moballegh, A.; Cao, Y.; Klein, A.; Dickey, E. C.; Irving, D. L.; Randall, C. A.; Chen, L.-Q. Defect Chemistry and Resistance Degradation in Fe-Doped SrTiO3 Single Crystal. Acta Mater. 2016, 108, 229−240.

[10]. Bayer, T. J. M.; Wang, J.-J.; Carter, J. J.; Moballegh, A.; Baker, J.; Irving, D. L.; Dickey, E. C.; Chen, L.-Q.; Randall, C. A. The Relation of Electrical Conductivity Profiles and Modulus Data Using the Example of STO:Fe Single Crystals: A Path to Improve the Model of Resistance Degradation. Acta Mater. 2016, 117, 252−261.

[11]. Kwon, D.-H.; Lee, S.; Kang, C. S.; Choi, Y. S.; Kang, S. J.; Cho, H. L.; Sohn, W.; Jo, J.; Lee, S.-Y.; Oh, K. H.; Noh, T. W.; De Souza, R. A.; Martin, M.; Kim, M. Unraveling the Origin and Mechanism of Nanofilament Formation in Polycrystalline SrTiO3 Resistive Switching Memories. Adv. Mater. 2019, 31, 1901322.

[12]. Du, H.; Jia, C.-L.; Houben, L.; Metlenko, V.; De Souza, R. A.; Waser, R.; Mayer, J. Atomic Structure and Chemistry of

Dislocation Cores at Low-Angle Tilt Grain Boundary in SrTiO3 Bicrystals. Acta Mater. 2015, 89, 344−351.

[13]. Gao, P.; Ishikawa, R.; Feng, B.; Kumamoto, A.; Shibata, N.; Ikuhara, Y. Atomic-Scale Structure Relaxation, Chemistry and Charge Distribution of Dislocation Cores in SrTiO3. Ultramicroscopy 2018, 184, 217−224.

[14]. Otsuka, K.; Kuwabara, A.; Nakamura, A.; Yamamoto, T.; Matsunaga, K.; Ikuhara, Y. Dislocation-Enhanced Ionic Conductivity of Yttria-Stabilized Zirconia. Appl. Phys. Lett. 2003, 82, 877−879.

[15]. Maras, E.; Saito, M.; Inoue, K.; Jonsson, H.; Ikuhara, Y.; McKenna, K. P. Determination of the Structure and Properties of an Edge Dislocation in Rutile TiO2. Acta Mater. 2019, 163, 199−207.